Asian Journal of Chemistry; Vol. 34, No. 11 (2022), 2975-2983

ASIAN JOURNAL OF CHEMISTRY

https://doi.org/10.14233/ajchem.2022.23973

Investigation of Dual Redox Electrolyte based on 1,1′-Dimethyl-4,4′-bipyridinium Diiodide for Superior Supercapacitors

S. LALITHA[1], A.M. SHANMUGHARAJ[2], R.A. KALAIVANI[1], M. SELVAKUMAR[3] and S. RAGHU[2,*]

[1]Department of Chemistry, Vels Institute of Science, Technology & Advanced Studies (VISTAS), Chennai-600117, India
[2]Centre for Advanced Research & Development (CARD), Department of Chemistry, Vels Institute of Science, Technology & Advanced Studies (VISTAS), Chennai-600117, India
[3]Department of Chemistry, Manipal Institute of Technology, Manipal Academy of Higher Education, Manipal-576104, India

*Corresponding author: E-mail: subraghu_0612@yahoo.co.in

Received: 18 June 2022; *Accepted*: 1 September 2022; *Published online*: 19 October 2022; AJC-21016

Development of more energy-efficient storage systems is required to meet the growing worldwide demand for energy. Redox electrolytes are clearly a long-term choice for high-energy-density supercapacitor applications in near future. Herein, the synthesis and electrochemical investigations of a dual redox electrolyte based on 1,1′-dimethyl-4,4′-bipyridinium diiodide as high-performance supercapacitors are reported. Previous researchers have focused on methyl viologen with reduced and oxidized redox bromide additive electrolytes at the negative and positive electrodes, respectively. In this work, by replacing iodine with bromine to solve current collector issues, reduce corrosion and contribute to the low toxic impact on the environment is investigated. The electrochemical results revealed that the maximum energy density of 63 Wh kg^{-1} and the capacity of 514 F g^{-1} were achieved with a modest concentration of additives. Exclusively, iodide anion boosted the stability by 95% and reduced deterioration until 10,000 cycles. This ground-breaking idea addresses the development of high-energy-density supercapacitors as well as a viable energy storage approach.

Keywords: Supercapacitor, Dual redox electrolyte, Energy storage, pseudocapacitance, Corrosion inhibition.

INTRODUCTION

The world is facing a challenging era in need of clean and green energy alternatives. Innovative and efficient energy storage systems are essential components to build robust scientific and industrial foundations. As a consequence, supercapacitors have attracted a lot of attention owing to their extraordinary power density and rate capacity, ultra-long cycle life and inexpensive maintenance [1]. According to their charge storage systems they store charge in two ways (i) EDL capacitance (EDLC) and (ii) pseudocapacitance. EDLC is due to the electrostatic separation which takes place between ionic and electronic charges at the interface of electrolyte and electrode surface, whereas pseudocapacitance is associated with rapid Faradaic processes at the electrode surface (redox/charge transfer process) [2].

Highly porous electrode materials with high surface area and strong electrical conductivity is necessary to improve the energy density of the supercapacitor. Carbon-based materials like activated and mesoporous carbon, graphene and carbon nanotubes (CNTs) have been employed as electrode materials in electric vehicles to investigate EDLC performance [3]. In commercial supercapacitors, activated carbon is a frequently used electrode material. Inspite of its enhanced specific surface area ranging from 500 to 2500 m^2 g^{-1} activated carbon is only applicable to a minimal extent in energy storage applications. This is due to the unpredictability of activated carbon compounds that arise in terms of micropores isolated from the electrolyte solution and these macropores result in lowering the surface-volume ratio makes the poor specific capacitance [4].

The choice of an appropriate electrolyte is a key aspect in improving the electrochemical performance of supercapacitors and achieving higher specific capacitance values. Electrolytes have the potential to influence ultimate device performance by altering the operational potential window. The optimization of electrode-electrolyte compatibility has been the topic of many earlier investigations [5]. A new approach for injecting modest amounts of single redox active compounds into the electrolyte

has been devised recently. Organic molecules with neutral redox activity such as *p*-phenylenediamine, poly-(*p*-phenylenediamine), *m*-phenylenediamine, quinone (or) hydroquinone, anthraquinone, anthraquinone-2,7-disulphonate, methylene blue, indigo carmine, *etc*. and ionic redox active species like $VOSO_4$, $CuCl_2$, iodide, bromide, *etc*. have been employed in EDLCs as redox additives [6]. Through pseudocapacitance arising from their reversible redox reaction, redox additives considerably improves the specific energy and specific capacitance of EDLCs. Recent study suggests that on both positive and negative electrodes these redox additives have exceptional redox active behaviour [7]. Redox additives based on halides are better for the positive electrode in comparison with the negative electrode since pseudocapacitance considerably improves the efficacy of the positive electrode [7,8]. To overcome these drawbacks, Frackowiak *et al.* [2] investigated a single SC with respect to the synergic effect of potassium iodide and $VOSO_4$ where they acted as the positive and negative electrode compartments of the EDLC, respectively. Similarly, Zhong *et al.* [9] emphasized a single device with a combination of two gel-polymer electrolytes comprising of methylene blue and hydroquinone redox additives. Both the studies used an expensive ion selective membrane (nafion) to divide the oppositely charged compartments. Zhong *et al.* [9], on the other hand, explored the use of a gel polymer electrolyte/H_2SO_4 medium based on polyvinyl to study the synergic effect between KI and $VOSO_4$ in the absence of a separator. Sang-Eun-Chun *et al.* [10] also reported the study on impact of KBr and methyl viologen bromide (redox active additives) on the specific capacitance and energy density of the EDLC. The results revealed that the combination of a cationic and an anionic redox active additive significantly increased the performing capacity of an EDLC when compared to a solo redox additive EDLC. Unlike the previous research works on redox additives, viologen's redox potential can be tuned by changing its alkyl groups [11]. Thus, it is essential to explore their effects for the commercialization of redox electrolyte-based supercapacitors in the near future.

In this work, we have incorporated 1,1′-dimethyl-4,4′-bipyridinium diiodide (referred as methyl viologen diiodide, MVI_2) to develop a redox additive and redox active species in the electrolyte (KI). Since, KI is a non-toxic, ecologically acceptable redox active species that prevents the corrosion of current collectors. It can potentially create distinct redox pairs of iodide on the electrode surface and improve the capacitance of the devices [12]. Due to its exclusive electron transfer performance, MVI_2 is widely used in solar cells, fuel cells, sensors, electrochromic and nano-electronic devices as an active redox material. In contrast to prior studies that used bromide as a redox addition, we used iodide instead of bromide in order to reduce corrosion and less toxic to the environment. Iodide anions have been found to significantly improve the inhibitive performance of metal surfaces in several studies [13-15]. As stated by Umoren *et al*. [16], the chemisorption resulted in decreased repulsive effect of metal ions over inhibitor molecules. These molecules (cation species) have specific functional groups that are readily prone to protonation and form an excessive cloud of electrons over the metal surface. The electron cloud thus formed attracts the cation species leading to the metal surface being masked and secured from destructive agents of the corrosive environment.

Based on these facts, the use of MVI_2/KI as a dual redox species for supercapacitors is presented in this article. The pseudocapacitance generated by the reversible Faradic interaction of bipyridinium cation and I^- anion increases the performance of both negative and positive electrodes at the same time. Over 10,000 cycles, a device using KI (3.5 M)/MVI_2 (0.1 M) delivers energy density of 63 Wh kg^{-1} at a specific power of 3150 W kg^{-1} with negligible fading. The cyclic voltammetry (CV), galvanostatic charge-discharge (GCD) and electrochemical impedance spectroscopy (EIS) techniques were used to evaluate the supercapacitor's electrochemical performance.

EXPERIMENTAL

Iodomethane, 4,4′-bipyridine, potassium iodide and acetone were purchased from Sigma-Aldrich, USA. Activated carbon, conductive carbon and Teflon binder were also procured from Sigma-Aldrich, USA. The Fourier transform infrared, nuclear magnetic resonance and mass spectroscopies were used to characterize the produced redox electrolyte. A two electrode coin cell setup was used to examine the materials for their electrochemical characteristics. The cyclic voltammetry, electrochemical impedance spectroscopy, galvanostatic charge/discharge and cycling performance were used to assess the electrochemical properties of the produced redox electrolyte. Milli-Q water was used throughout to make all of the solutions.

Synthesis of redox electrolyte (MVI_2): 4,4′-Bipyridine (1.9 g) was dissolved in 20 mL of acetone under magnetic agitation. Iodomethane (3.52 mL) was added dropwise to the agitating solution. Under nitrogen atmosphere and water cooled reflux the reaction mixture was agitated at 80 ºC for 24 h. Monomethyl viologen (MVI) was obtained as an orange precipitate, filtered and washed with acetone several times to eliminate any unreacted 4,4′-bipyridine. The MVI_2 was obtained with a yield of 73 mol% (3.95 g) (**Scheme-I**). Other viologens were synthesized in the same way and employed as an electrolyte for super capacitor applications.

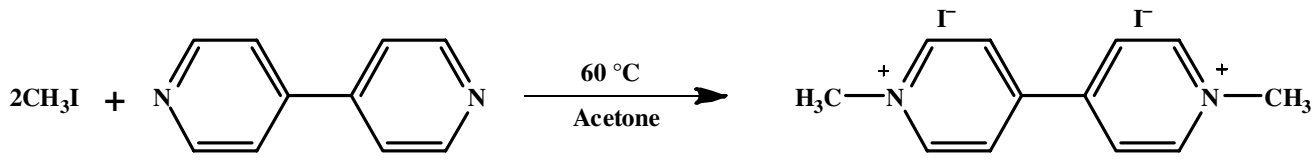

Methyl iodide **4,4'-Bipyridine** **Methyl viologen diiodide**

Scheme-I: Synthesis of methyl viologen diiodide (MVI_2)

Fabrication of electrodes/electrolyte/symmetric supercapacitor: A self-standing carbon film electrode for the symmetric coin cell electrode system was prepared by homogeneously combining 85% activated carbon, 10% conductive carbon and 5% Teflon binder. The resulting paste was calendared into a film and dried at 120 ºC for 2 h in a vacuum oven. After weighing, the mass of the electrode was found to be around 5-8 mg/electrode. Finally, the coin cell electrode was assembled with activated carbon sheet (anode and cathode) and electrolyte (3.5 M KI with 0.1 M MVI_2) with a Whatmann-Glass fibre separator.

RESULTS AND DISCUSSION

Electrochemical characterization: Using a two/three electrode system, the electrochemical performance of redox electrolyte (MVI_2/KI) and pristine electrolyte (KI) was investigated using cyclic voltammetry (CV), galvanostatic charge-discharge (GCD) and electrochemical impedance spectroscopy (EIS) techniques. For the three electrode system, commercial activated carbon film was used as the working and counter electrodes with Ag/AgCl as the reference electrode whereas for the two electrode system, activated carbon was used as the anode and cathode with 3.5 M KI and 0.1 M MVI_2 as the electrolyte. Impedance measurements were performed at AC voltage of 10 mV amplitude in an open circuit voltage working at a frequency range of 1 Hz to 105 Hz (OCV). Biological SP-300 instrument and neware battery tester were used for all electrochemical parameters, which were performed at room temperature.

The specific capacitances can be calculated from eqn. 1:

$$E = \frac{I \times \Delta t}{m / \Delta V} \quad (1)$$

where I = constant discharge current, Δt = discharging time, m = mass of one electrode and ΔV = voltage drop upon discharging.

Energy density (E) and power density (P) can be calculated from eqns. 2 and 3:

$$E = \frac{1}{2} CV^2 \quad (2)$$

$$P = E \times \frac{3600}{t} \quad (3)$$

where E, C, V, P and t are the specific energy, specific capacitance, potential window, specific power and discharge time, respectively [17].

FT-IR studies: Table-1 show the FT-I R spectra of MVI_2 and its matched IR peak positions. The -CH asymmetric and symmetric stretching vibrations of arom.-CH and aliph.-CH_3 groups of MVI_2 are attributed due to the broad intense doublet peaks at 3083 and 2950 cm^{-1}, as well as the sharp peak at 2850 cm^{-1}. Existence of the aromatic -CH and aliph.-CH_3 groups are confirmed by the out-of-plane bending (1455 cm^{-1}), wagging (1348 cm^{-1}) and scissoring (1118 cm^{-1}) vibrations. Stretching vibrations of the aromatic carbon atoms (including C=C *str.*) in the pyridinic structures of MVI_2 are responsible for the series of peaks in the spectral range 1600-1500 cm^{-1}. The aromatic characteristics is further supported by the existence of overtones and combination bands at 2500 cm^{-1} (Fig. 1).

TABLE-1
FT-IR SPECTROSCOPY ABSORPTION OF FREQUENCY REGIONS OF DUAL REDOX ELECTROLYTE (METHYL VIOLOGEN DIIODIDE)

V_{obs}	Approximate descriptions
467	Ring-ring stretch
704	C–N–CH_3 in-plane bending
784, 812	Ring deformations + in-plane bending
836	N^+–CH_3 stretch
953	Ring breathing
1432	Heterocyclic C–C stretch
1455	H–C–H twist
3083	Aromatic C–H stretch

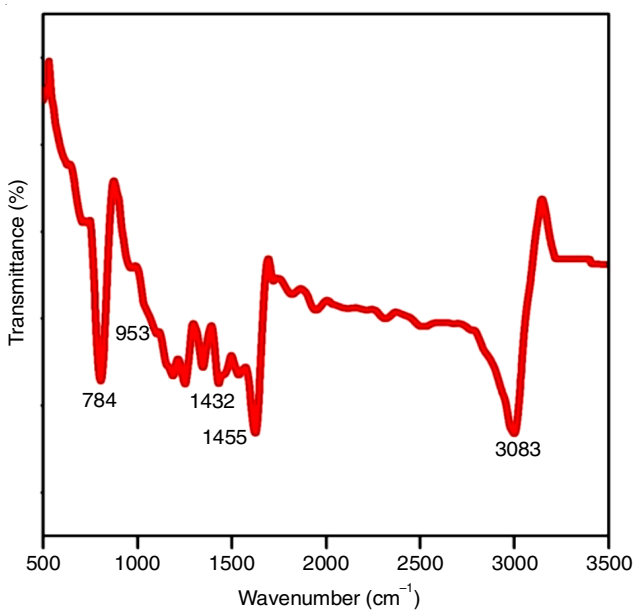

Fig. 1. FT-IR spectroscopy for methyl viologen diiodide redox electrolyte

Presence of aromatic bipyridyl rings may be seen by the distinctive medium absorption peaks at 1267 and 1226 cm^{-1}, attributable to C-N stretching. The presence of a modest absorption bands between 800 and 900 cm^{-1} (N^+-CH_3 stretching) confirms the quaternary character of the nitrogen in MVI_2. The above fact is strengthened by absorption bands at 704 and 784 cm^{-1}, which resemble the in-plane bending vibrations of the C-N-CH_3 group. The ring-ring stretching vibrations of bipyridyl groups in MVI_2 can be connected to the medium absorption peak at 467 cm^{-1}.

NMR studies: In relevance to the schematic representation shown in Fig. 2a-b, protons 1a, 5a, 9a and 11a are in the same environment and produce a doublet peak at δ 8.9 ppm shift value. Similarly protons 8a, 12a, 2a, 4a produce another doublet peak at δ 8.2 ppm confirming the structure. The intensity ratio (1.25:1.2) is almost alike and signifies that the proton exists in 1:1 ratio and further supports the structure proposed in the schematic representation. In addition a singlet peak at δ 4.6 ppm corresponds to the six protons of the methyl groups attached to the nitrogen atom of pyridyl groups.

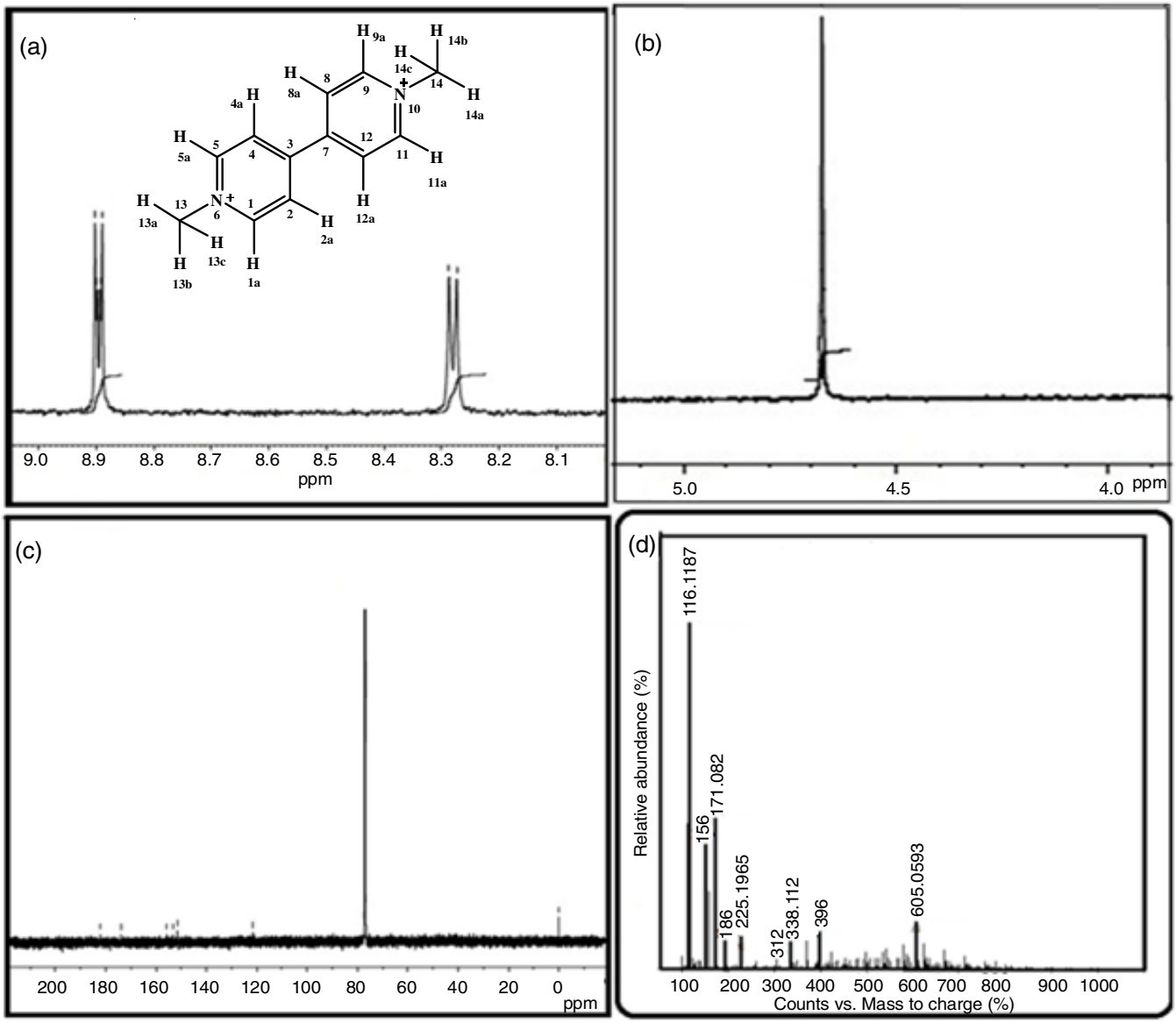

Fig. 2. Representation of (a,b): ^{1}H NMR spectrum (c) C^{13} NMR spectrum (d) Mass spectroscopy of methyl-viologen diiodide redox electrolyte

In ^{13}C NMR spectra (Fig. 2c), a shift at ~ 153 ppm is confirmed to the four tertiary carbon atoms (C1, 5, 9 and 11) closer to the nitrogen atom of the bipyridyl rings. The presence of the enantiomeric form of the structure is indicated by the formation of adjacent peaks closer to 153 ppm. The peak shift at ~ 173 ppm can be correlated to the C-C bond (C3 and 7) between the bipyridyl rings [18].

Mass studies: A molecular ion peak at *m/z* = 338 is assigned to 1,1′-dimethyl-4,4′-bipyridiniumdiiodide. After one molecule of iodine elimination the peak was observed at *m/z* =312 (1,1′-dimethyl-4,4′-bipyridiniumiodide). On the elimination of two molecules of iodine the *m/z* ratio was 186 (1,1′-dimethyl-4,4′-bipyridiniumcation). Then the peak was observed at 171 is MV^{+}. The fragment at *m/z* = 156 is related to bipyridinium cation and *m/z* = 116 is related to 1-cyclopropylpyridine [19].

Electrochemical characterization of redox electrolyte: The present study discusses about the dual redox electrolyte (MVI_2/KI) and the formation of MV^{2+}/MV^{+} redox couple that enhance the pseudocapacitive contribution at the electrode surface. The composition of the redox active electrolyte was optimized on the basis of some preliminary investigations (S1). Primarily, a pristine electrolyte (KI) with various molar concentrations (1 to 5 M) was prepared and checked. After that varied concentrations of redox active species (MVI_2) were added. Fig. 3a shows the graph shows the relationship between ionic conductance and electrolyte concentration. According to the results, 3.5 M KI with 0.01 M MVI_2 produced a high ionic conductance when compared to the other combinations. The optimized ionic conductivity experiment revealed that the diluted solution of methyl viologen-based organic salts has excellent conductivity indicating the high mobility of MV^{2+} anion counter. The initial conductivity study indicated that 3.5 M KI with 0.1 M MVI_2 is the best redox electrolyte concentration for supercapacitor applications.

Fig. 3b depicted the charge and discharge curves for MVI_2/KI at various voltages. The use of redox additive electrolytes

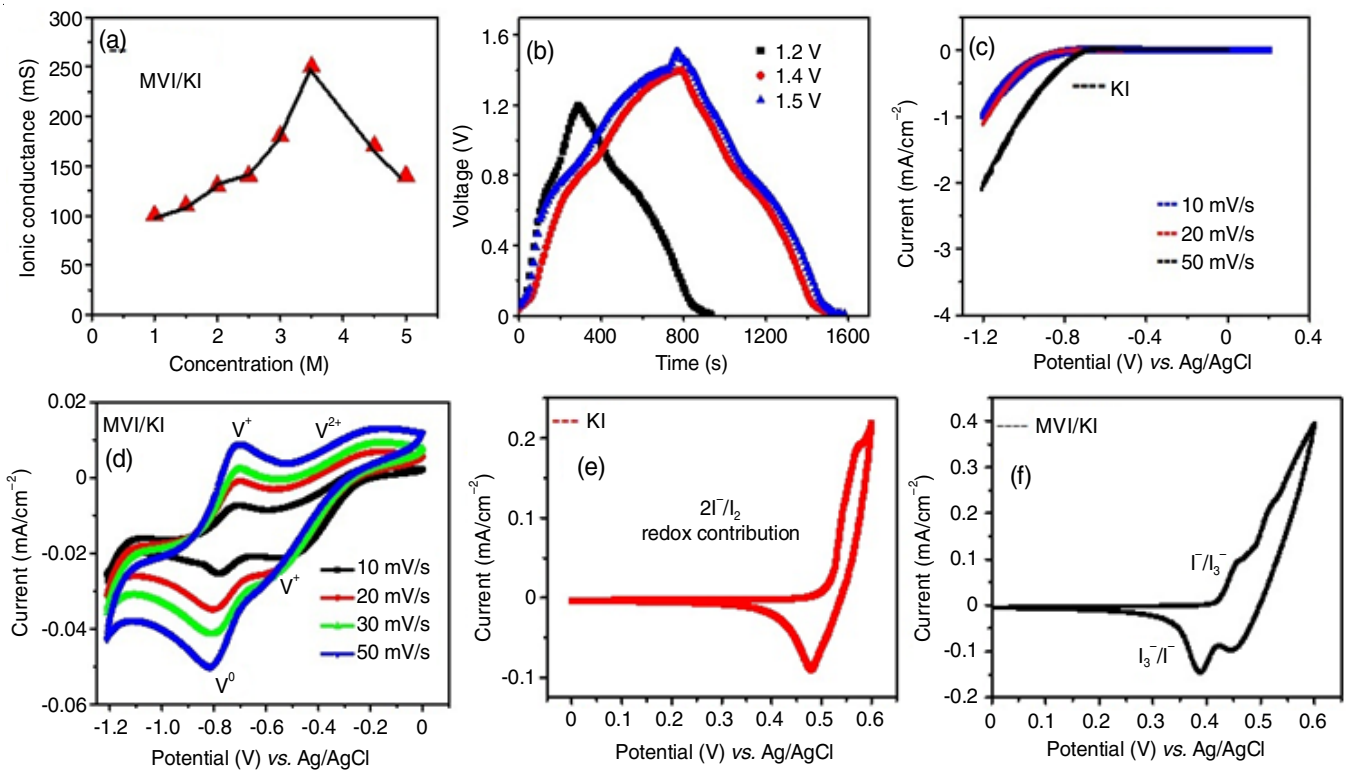

Fig. 3. Representation of (a) ionic conductance with respect to concentration of the electrolyte, (b) charge-discharge curve at different voltages, (c,d) CV under negative and positive potential of 0.1 M KI in MVI_2 at 20 mV s^{-1}, respectively and (e,f) CV under positive potential in presence of redox electrolyte (KI) and redox additive aqueous electrolyte (MVI/KI), repectively

in supercapacitors has been proposed to provide a wider range of potential window than conventional aqueous electrolytes. After confirming the redox behaviour of electrolyte at various voltages ranging from 1.2 V to 1.5 V, the voltage for the redox electrolyte was set at 1.4 V. According to the results, the charging curve hump is near 0.5 V (1.2 V, 1.4 V and 1.5V) and the discharging curve hump is near 0.75V. It is observed that on increasing the voltage for dual redox electrolyte the pseudo capacitive contribution of bipyridinium cation and iodide anion is reduced.

Fig. 3c-d showed the cyclic voltammetry experiments conducted under mixtures of dual redox aqueous electrolyte (MVI_2/KI) for both positive and negative sides. Fig. 3e-f represents the CV at positive potential under single redox electrolyte (KI) and in the presence of MVI/KI, where in the presence of single redox electrolyte of KI did not show any peak in the negative side but dual redox electrolyte showed two sets of redox peaks in the reduction and oxidation sides. This redox peak confirms the possible valence states to be MV^0/MV^+ and MV^+/MV^{2+}.

In Fig. 3d, the peaks II and II′ occured at -0.5 V and -0.8 V *vs*. Ag/AgCl were associated with the redox couple:

$$MV^{2+} + e^- \longrightarrow MV^+ \quad (1)$$

The second redox couple (peak I and I′) occuring at -0.4 V and -0.7 V *vs*. Ag/AgCl exhibited a diffusion controlled voltammetric behaviour corresponding to the process generating neutral molecules in solution.

$$MV^+ + e^- \longrightarrow MV^0 \quad (2)$$

As the potential sweep is extended to the oxidation regime, two peaks 2' and 1' at -0.5 V and -0.8 V occurred due to the following reactions:

$$MV^0 \rightleftharpoons MV^{+\bullet} + e^- \quad \text{Peak 2'} \quad (3)$$

$$MV^{2+} \rightleftharpoons MV^+ + e^- \quad \text{Peak 1'} \quad (4)$$

The occurrence of reversible peaks in the redox-mediated electrolyte confirmed the pseudocapacitive behaviour, which arise from the Faradaic reaction of redox additive electrolyte. To determine whether the reaction is diffusion or adsorption controlled, the dual redox electrolyte solution was studied at various scan rates (10 to 50 mV s^{-1}) in the potential range of 0.2 V to -1.2 V (Fig. 3d). When the scan rate was increased the redox electrolyte's reduction potential slightly shifted with the peak current. One of the common characteristics of quasi-reversible electrodes is the shifting of oxidation/reduction potential peaks as scan rates increases. Thus, the behaviour of the electrolyte corresponded to a typical quasi-reversible redox process. Even after the addition of redox additives (MVI_2) and increasing the scan rate the peak shift was only minimal. Also, when the scan rate was increased the area under the curve became larger. Voltammograms of MVI_2/KI at different scan rates revealed the excellent pseudocapacitive contribution of aqueous redox additive electrolyte. However, as the scan rate increased the onset of bipyridinium cation reduction shifted towards a lesser positive potential. Thus, the decrease in the cation's pseudo capacitive contribution at higher scan rates is confirmed as the peak maxima was not reached in the working potential limit.

The galvanostatic charge and discharge curves of a dual redox electrolyte (MVI_2/KI) and electrolyte (KI) were tested under a constant voltage (0-1.4 V) at different current densities. The graph was linear up to 0.5 V and began to deviate slope from 0.5 V to 0.75 V before returning to linear (Fig. 4a-b). The ionic contribution of bipyridinium cation and iodide ion are possibly responsible for the slope deviation. Due to this additional ionic contribution of the redox electrolyte the charging and discharging time was increased. The dual redox electrolyte's charging and discharging times were found to be nearly identical (790 s and 730 s) and the IR drop is around 0.017 V. From the time *vs.* voltage graph (Fig. 4a-b), it can be seen that the electrolyte has a high conductivity. The coulombic or capacitance efficiency of the dual redox electrolyte was 92.14% and MVI_2/KI had a high symmetric charge-discharge curve indicating good reversibility. At varied current densities, the time limit of MVI_2/KI was longer (1520 s) than that of pristine electrolyte (800 s) (Fig. 4b). Additionally, there was no significant IR drop observed. The longer discharge time of MVI_2/KI demonstrated the electrolyte's good ionic conductivity and diffusion contribution which will directly increase the system's capacity. Nevertheless, a symmetric isosceles triangle was seen for the pristine electrolyte (Fig. 4b).

A galvanostatic charge-discharge was performed in a range of current densities from 1 A g^{-1} to 10 A g^{-1} to assess the rate capacity of the supercapacitor. The charge discharge profile for dual redox electrolyte and pristine electrolyte was plotted as a function of capacitance *versus* voltage (Fig. 4c-d). Even at higher current densities highly symmetric shapes (10 A g^{-1}) were exhibited. Fig. 4d depicts the charge-discharge profile for a dual redox electrolyte. In the charging and discharging process, a plateau redox behaviour was evidenced at 0.4 to 0.9 V. The slope of the graph deviates from 0.4 V to 0.8 V and deviates once again at 0.9 V resulting in a shape change to linear at 1.1 V (hump was observed). The graph was similar to that of MVI_2/KI's CV graph. When methyl viologen redox species was added the discharging time nearly doubled for all current densities. The capacitance for pristine electrolyte were nearly 265, 180, 67 and 27 F g^{-1} at 1, 2, 5 and 10 A g^{-1} as showed in Fig. 4c. In the case of dual redox electrolytes (Fig. 4d) capacitances of 514, 337, 199 and 99 F g^{-1} at 1, 2, 5 and 10 A g^{-1} were found. The dual redox electrolyte's initial capacity was 514 F g^{-1} at 1 A g^{-1} and declined to 99 F g^{-1} at 10 A g^{-1}. Entirely, when compared to pure KI redox electrolyte, the capacitance values were nearly doubled.

The degradation studies for dual redox electrolyte and pristine electrolyte at 1 A g^{-1} in a two-electrode system (coin

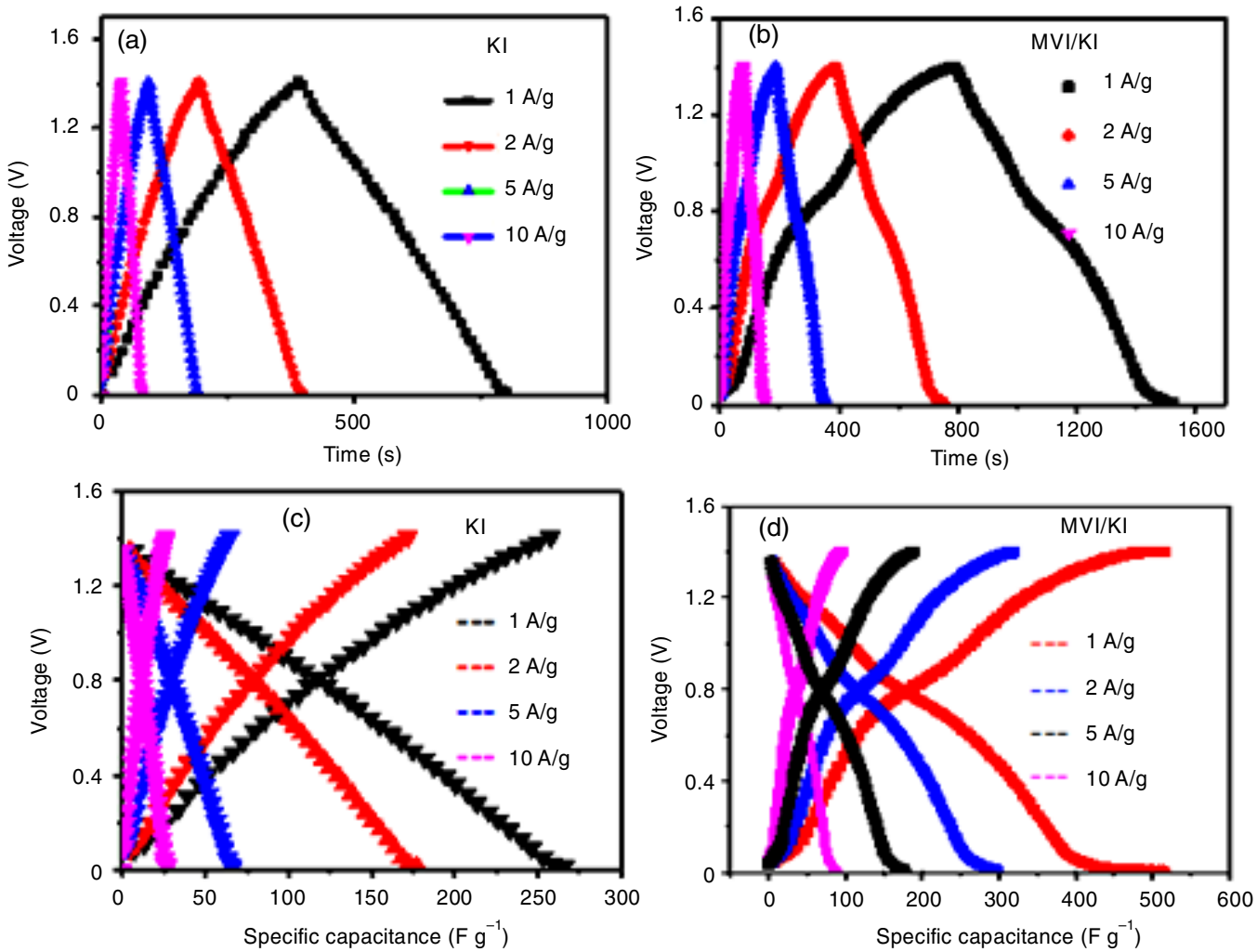

Fig. 4. Representation of GCD in the presence of (a,c) KI (b,d) MVI/KI electrolyte at different current density and capacitance

cell) are displayed in Fig. 5a. The pristine electrolyte's capacitance began with greater stability but after 1000 cycles it starts to decrease. Yet, it was observed to become very stable after 4000 to 6000 cycles. Despite this behaviour, 85% of the initial capacitance was preserved after 10,000 cycles. The overall capacitance value for dual redox electrolytes on the other hand is slightly larger in the beginning and its capacitance remained relatively consistent over time. This behaviour could be explained by the delayed migration of bipyridinium cations. After 10,000 cycles, it was found to preserve roughly 92.40% of its initial capacitance. Based on these results, addition of methyl viologen to the electrolyte enhances the capacitance and retains it steady for 10,000 cycles. The rate performance for both of the electrolyte is represented in Fig. 5b, and it is found that the initial capacitance of dual redox electrolyte (MVI_2/KI) and pristine electrolyte at 1 A g^{-1} current density are approximately 514.46 and 265.74 F g^{-1}, respectively. These capacity values were reduced to 337.15, 199.79 and 99.89 F g^{-1} for dual redox electrolyte and 180.49, 67.68 and 27.07 F g^{-1} for pristine electrolyte on increasing the current density to 2, 5 or 10 A g^{-1}. Thus, in comparison to pristine electrolyte (KI), dual redox electrolyte had twice the capacitance value 514.46 F g^{-1} at 1 A g^{-1} current density.

Energy and power density are two main parameters that are used to describe the performance of a supercapacitor. Fig. 5c represented the Ragone plot, which showed the energy and power densities of redox electrolyte (MVI_2/KI) and pristine electrolyte (KI) at various current densities. It is self-evident that when power density increases the energy density drops. The highest energy density of a supercapacitor is estimated as 63.32 Wh kg^{-1}. At greater current densities it decreases to 12 Wh kg^{-1} and rises about 0.73 to 3.15 Wh kg^{-1} on moving towards higher power densities. Most aqueous supercapacitors have values that are significantly lower than this. The maximum energy and power density of a supercapacitor achieved for the blank electrolyte at 1 A g^{-1} was 32 Wh kg^{-1} and 0.53 kW kg^{-1}, which decreased to 3 Wh kg^{-1} and 0.44 kW kg^{-1} on higher current density 10 A g^{-1}. Dual redox electrolyte's extraordinary

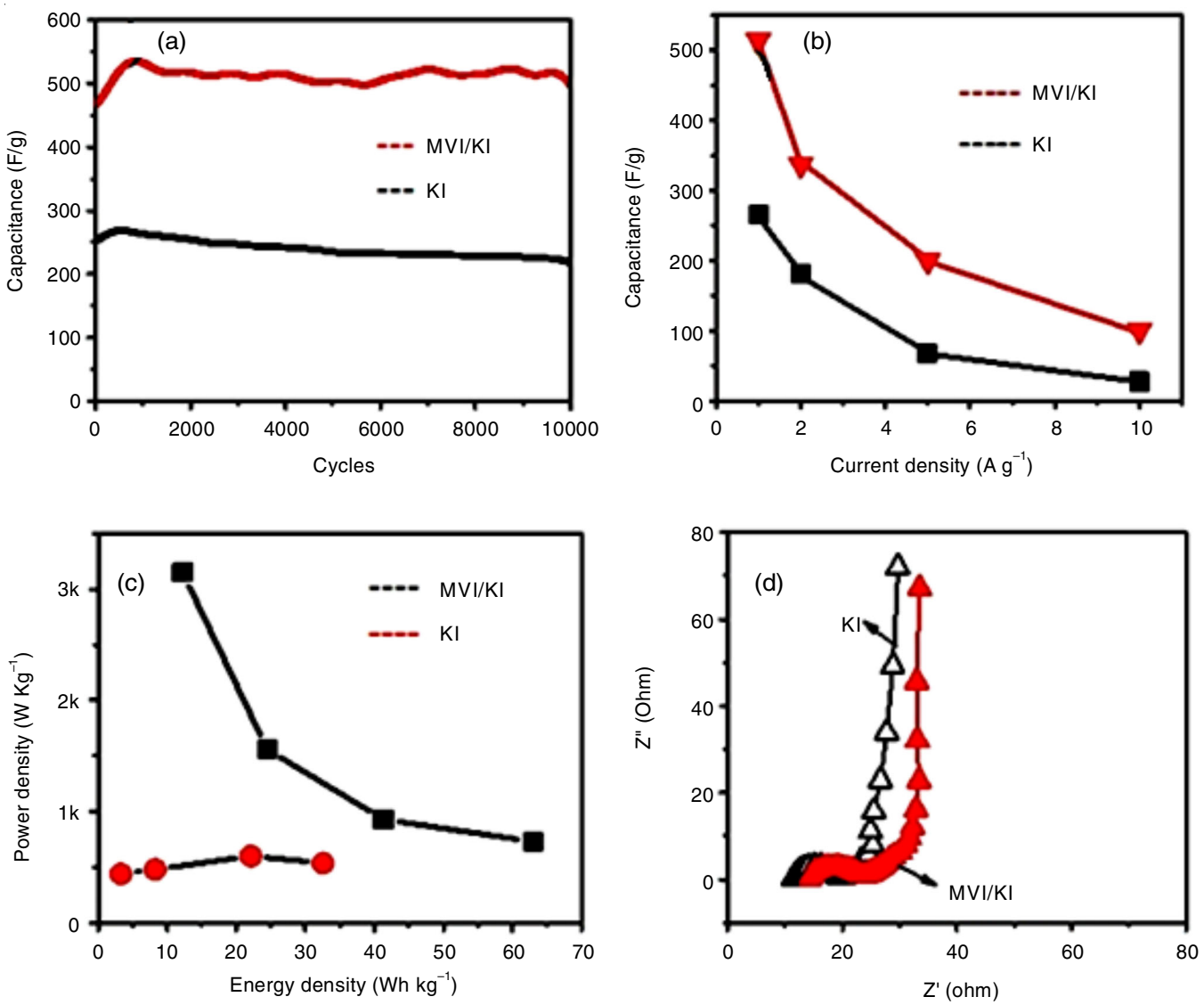

Fig. 5. Representation of (a) cycling stability (b) rate performance as current density *vs*. capacitances (c) Ragone plot and (d) Nyquist impedance plot (inset: corresponding equivalent circuit) for KI and MVI/KI electrolyte

energy and power density values suggests that it could be applicable in high performance supercapacitors application.

The EIS technique was investigated to understand the conductivity and ionic resistance of the dual redox electrolyte. At high frequency region the plots exposed a semicircle and at low frequency region it showed a straight line (Fig. 5d). The R_{ct} of the pristine resistance and dual redox electrolyte were calculated and found to be ~ 12 Ω and ~10 Ω, which shows that dual redox electrolyte has lower resistance than the pristine electrolyte. These results attributes to the dual redox electrolyte, which has significant performance than the pristine electrolyte and also these findings were in agreement with the cyclic voltammetry (CV) and galvanostatic charge-discharge (GCD) results.

Corrosion inhibition: A standard three electrode system was used to analyze the EIS measurements. A stainless-steel rod with a 1 cm^2 exposed surface area was dipped in the electrolyte solution (KBr and KI). Saturated Ag/AgCl and platinum acted as the reference and counter electrodes. Corrosion experiments were carried out using $MVBr_2$ and MVI_2 electrolytes. Impedance measurements were taken at the corrosion potential (E_{corr}) in the frequency range of 100 kHz-100100 mHz with 10 mV signal amplitude perturbation.

Inhibition efficiency (η_{EIS}) can be calculated by the following equation:

$$\eta_{EIS}\ (\%) = \frac{R_t - R_t}{R} \times 100$$

The EIS plot for stainless steel (SS) corrosion in $MVBr_2$/KBr and MVI_2/KI is depicted in Fig. 6a, which represents the Nyquist impedance and bode modulus. On examining the two redox electrolytes, the addition of I^- ions (MVI_2/KI) revealed the good capacitive loops and the low frequency magnitude of the bode modulus.This indicates that the MVI_2/KI redox electrolyte has a greater ability to inhibit corrosion. In the presence of KI, the solution resistance decreased while the charge transfer resistance increased. Thus, the addition of KI reduces the corrosion rate significantly.

When KI comes into contact with a metal surface, the I^- ions were adsorbed on the anode of the metal surface causing the surface charge to become negative. This happens due to the specific adsorption of these ions resulting in electron pair bonding with the metal surface. Bode [Z] plot exhibited the changes in absolute impedance and phase angle as a function of frequency. Fig. 6b showed the angle plots for the redox electrolytes. The phase angle of MVI_2/KI is close to 90º indicating that the device performs similarly to an ideal capacitor. Then, the cation species is attracted to the metal surface by the electron cloud on the metal surface, which resulted in wrapping and protecting from the destructive agents of the corrosive environment.

Conclusion

In summary, the electrochemical investigation of a novel dual redox electrolyte based on 1,1′-dimethyl-4,4′-bipyridinium diiodide for high-performance supercapacitors was discussed. The fabricated supercapacitor device with the novel electrolyte system combines both the energy-storage process such as EDLC formation and pseudo-capacitor process. The electrolyte system represents a significant advancement in the evolution of supercapacitors as it acts as an extremely efficient aid for increasing the electrical energy storage. For viologen-iodide combinations, the maximum specific capacitance was exhibited 514 F g^{-1} with 63 Wh kg^{-1} energy density. Surprisingly, the interaction between viologen and the carbon surface resulted in selective surface adsorption of bipyridinium cation on the negative electrode and consequently improved the stable specific capacitance up to 10,000 cycles. This supercapacitor device with the prepared efficient and novel electrolyte system will be the potential tool for the future scope of the overall energy storage system with ultra-high energy efficient redox compound.

ACKNOWLEDGEMENTS

The authors gratefully acknowledge the financial support from (DST/TMD/MES/2K17/39G), New Delhi and Vels Institute

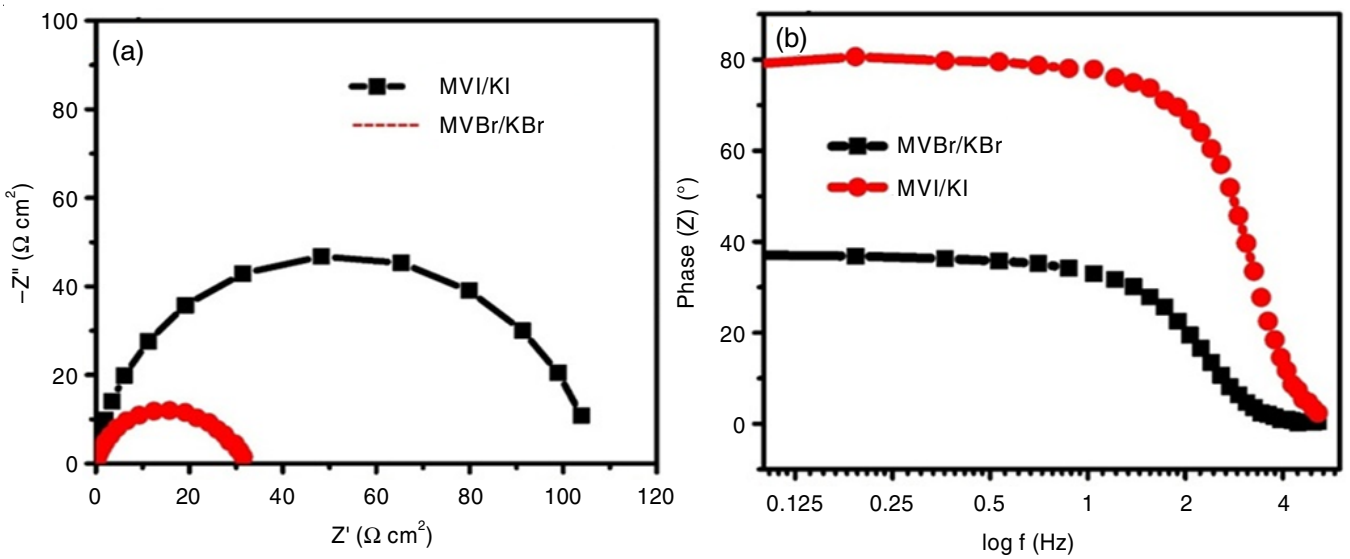

Fig. 6. (a) Nyquist impedance plot and (b) Bode plot for KI and MVI/KI, respectively

of Science, Technology & Advanced Studies (VISTAS), Chennai, India.

CONFLICT OF INTEREST

The authors declare that there is no conflict of interests regarding the publication of this article.

REFERENCES

1. L. Yan, D. Li, T. Yan, G. Chen, L. Shi, Z. An and D. Zhang, *Appl. Mater. Interfaces*, **10**, 42494 (2018); https://doi.org/10.1021/acsami.8b16642
2. E. Frackowiak, M. Meller, J. Menzel, D. Gastol and K. Fic, *Dominika Gasto and Krzyszt of Fic*, **172**, 179 (2014); https://doi.org/10.1039/C4FD00052H
3. Q. Sun, Y. Li and T. He, *J. Mater. Sci.*, **54**, 7665 (2019); https://doi.org/10.1007/s10853-019-03414-x
4. S. Sundriyal, V. Shrivastav, M. Sharma, S. Mishra and A. Deep, *ChemistrySelect*, **4**, 2585 (2019); https://doi.org/10.1002/slct.201900305
5. F. Zheng, Y. Yang and Q. Chen, *Nat. Commun.*, **5**, 5261 (2014); https://doi.org/10.1038/ncomms6261
6. R. Ramachandran, C. Zhao, D. Luo, K. Wang, F. Wang, *Electrochem. Acta*, **267**, 170 (2018); https://doi.org/10.1016/j.electacta.2018.02.074
7. S.T. Senthil Kumar, R. Kalaiselvan and J.S. Melo, *J. Mater. Chem. A*, **1**, 12386 (2013); https://doi.org/10.1039/c3ta11959a
8. S.T. Senthil Kumar, R. Kalaiselvan, M. Ulaganathan and J.S. Melo, *Electrochim. Acta*, **115**, 518 (2014); https://doi.org/10.1016/j.electacta.2013.10.199
9. J. Zhong, L.Q. Fan, X. Wu, J.-H. Wu, G.-J. Liu, J.-M. Lin, M.-L. Huang and Y.-L. Wei, *Electrochim. Acta*, **166**, 150 (2015); https://doi.org/10.1016/j.electacta.2015.03.114
10. S.-E. Chun, B. Evanko, X. Wang, D. Vonlanthen, X. Ji, G.D. Stucky and S.W. Boettcher, *Nat. Commun.*, **6**, 7818 (2015); https://doi.org/10.1038/ncomms8818
11. V. Presser, C.R. Dennison, J. Campos, K.W. Knehr, E.C. Kumbur and Y. Gogotsi, *Adv. Energy Mater.*, **2**, 895 (2012); https://doi.org/10.1002/aenm.201100768
12. H. Peng, G. Ma, K. Sun, J. Mu, X. Zhou and Z. Lei, *RSC Adv.*, **5**, 12034 (2015); https://doi.org/10.1039/C4RA11889H
13. R. Bhargava, T. Daeneke, S.J. Thompson, J. Lloyd, C.-A. Palma, J. Reichert, J.V. Barth, L. Spiccia and U. Bach, *J. Phys. Chem. C*, **119**, 19613 (2015); https://doi.org/10.1021/acs.jpcc.5b05195
14. A.A. Khadom, A.N. Abd and N.A. Ahmed, *J. Bio Tribocorros.*, **4**, 17 (2018); https://doi.org/10.1007/s40735-018-0133-4
15. W. Qin, N. Zhou, C. Wu, M. Xie, H. Sun, Y. Guo and L. Pan, *ACS Omega*, **5**, 3801 (2020); https://doi.org/10.1021/acsomega.9b04063
16. S.A. Umoren, U.M. Eduok, M.M. Solomon and A.P. Udoh, *Arabian J. Chem.*, **9**, S224 (2016); https://doi.org/10.1016/j.arabjc.2011.03.008
17. L. Han, H. Huang, X. Fu, J. Li, Z. Yang, X. Liu, L. Pan and M. Xu, *Chem. Eng. J.*, **392**, 123733 (2020); https://doi.org/10.1016/j.cej.2019.123733
18. X. Xu, J. Tang, H. Qian, S. Hou, Y. Bando, M.S.A. Hossain, L. Pan and Y. Yamauchi, *ACS Appl. Mater. Interfaces*, **9**, 38737 (2017); https://doi.org/10.1021/acsami.7b09944
19. L. Chen, X. Xu, L. Wan, G. Zhu, Y. Li, T. Lu, M.D. Albaqami, L. Pan and Y. Yamauchi, *Mater. Chem. Front.*, **5**, 3480 (2021); https://doi.org/10.1039/D0QM00946F